Response to RC2

We thank the reviewer for the helpful comments. Below we provide a detailed point-by-point response to the issues raised by the reviewer. Reviewer comments provided in *italics* and our responses follow in normal text. Changes to the manuscript are denoted in blue font. When our responses reference other comments, we use the formalism R#C#, such that R1C5 would refer to Comment 5 by Reviewer 1.

Comment #1

Page 4, Line 14: Were the aerosols dried prior to sampling? What was the average sample aerosol RH throughout the study? Were particle losses calculated for the PM1 to 2.5 range?

Response:

As indicated in Section 2.2.2 in the main text, "a Polytube Dryer Gas Sample Dryer (Perma Pure LLC) was mounted in front of the AMS inlet". The average RH is between 20% to 30% after the dryer. The AMS lens transmission efficiency of particles from 1 to 2.5 μm is approximately unity (Williams et al., 2013), therefore particle losses were not calculated.

Comment #2

Can the authors add the size range typically measured by the EESITOF to the discussion of particle size sampling efficiency on page 5/6.

Response:

The EESI-TOF measures particles up to at least 750 nm diameter with better than 80% efficiency (Lopez-Hilfiker et al., 2019). Recent work in our laboratory shows a significant increase in sensitivity below 100 nm (Lee et al,.2021), but due to the small mass fraction contained in this size range, this size dependence has a negligible effect on the current study. The EESI-TOF has not been characterised in the laboratory for particles larger than 750 nm, but given the absence of systematic differences in EESI-TOF vs. AMS comparisons for clean vs. haze periods, which have mode diameters of 302 and 665 nm (see Fig. S3), respectively, with a significant mass fraction above 1 μm during haze (see response to R2C4, R2C5, and Fig. S3), we expect that the AMS and EESI-TOF measure approximately the same size fraction (roughly $PM_{2.5}$).

Comment #3

How often was the denuder regenerated during the sampling campaign?

Response:

We utilised two denuders for the campaign, with one in operation while the other was regenerated in an oven at ~200 °C. Each denuder alternated 24 hrs of sampling with 24 hrs regeneration. We now note this in the text as follows (page 4 line 5):

"After sampling for 24 hrs, the denuder was replaced, and regenerated for 24 hrs in an oven at ~200 °C."

Comment #4

What is the make and model of the SMPS used in this study? What is the size range measured by the SMPS. Can the authors show the aerosol size distribution measured by the SMPS and compare with that of the L-TOF (shown in Fig S2).

Response:

We have added the following sentence to section 2.1 (page 3 line 32):

"A scanning mobility particle sizer (SMPS), consisting of a model 3080 DMA and model 3022 CPC (TSI, Inc., Shoreview, MN, USA), an aethalometer (model AE33, Magee Scientific, Ljubljana, Slovenia) and an Xact 625i Ambient Metals Monitor (Cooper Environmental Services LLC, Tigard, Oregon, USA) were additionally deployed at the site to measure the particle size distribution from 15.7 to 850.5 nm, the equivalent black carbon (eBC) concentration and the mass of 35 different elements in PM_{10} and $PM_{2.5}$, respectively."

We have added SMPS distributions to all plots of AMS size distributions. The figures below show the new Fig. S3a (average of all haze periods except 4 to 7 Nov.) and S3b (average of all clean periods). SMPS distributions are shown as mass distributions as a function of mobility diameter, with an effective density of 1.2 g cm^{-3} used to estimate mass.

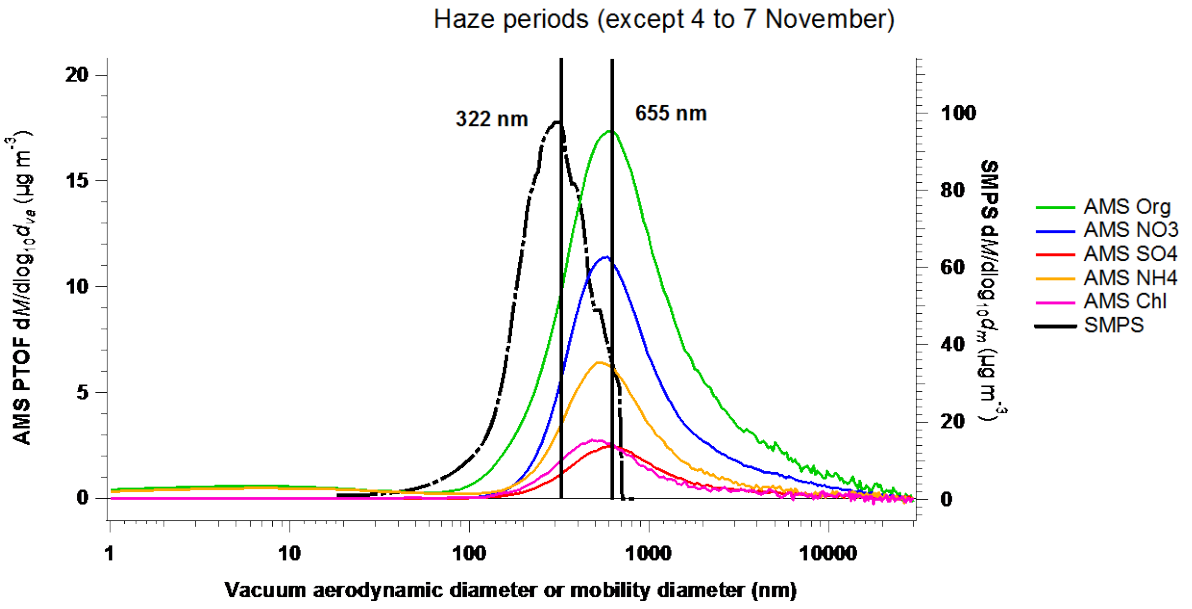

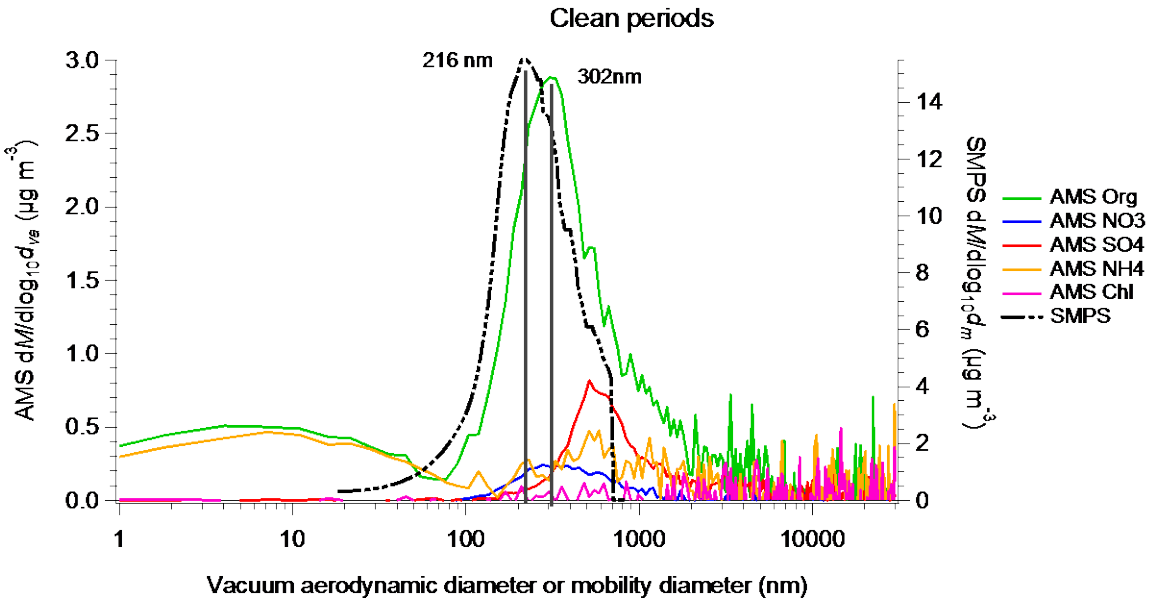

Comment #5

How did this size range change during the different sampling events "haze events" and the "clean periods" (Heating non-heating)?

Response:

Figure S3 (see response to previous comment) shows a mode vacuum aerodynamic diameter (d_{va}) of 302 nm for the clean periods and 665 nm for the haze episodes. Also of note, a significant fraction of mass occurs above 1 µm during haze, consistent with previous studies (Elser et al., 2016)

We have also added Figs. S3c-S3h to the supplement, which show SMPS and AMS size distributions for the following events: 10-11 Nov. (clean, non-heating), 22-24 Nov. (clean, heating), 11-13 Nov. (haze, non-heating), 30 Nov – 3 Dec (haze, heating), 4-7 Nov. (intense haze, non-heating, aqueous chemistry-influenced) and 18-22 Nov (intense haze, heating, strong SFC contribution). For clean periods, the the mode diameter during the non-heating season is larger than during the heating season. For haze periods, the mode diameters in the heating and non-heating seasons are usually comparable, with the exception of two severe haze events. These events, in which larger particles are observed are the 18 to 22 Nov severe haze characterised by biomass burning activity, and the aqueous chemistry-influenced severe haze from 4 to 7 Nov.

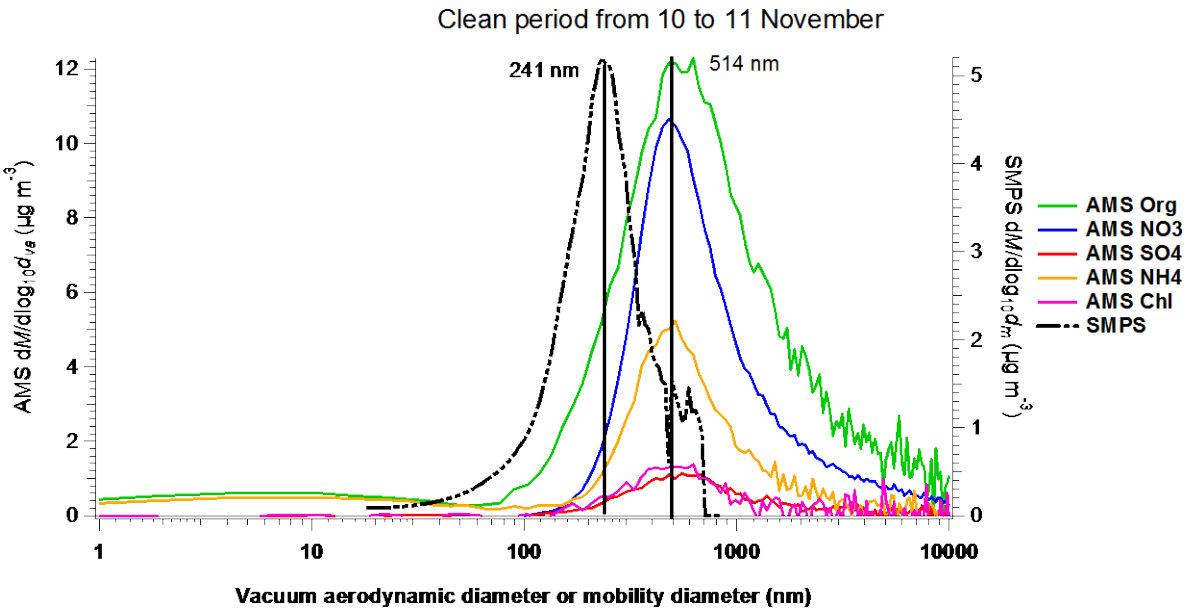
Clean period from 10 to 11 November
241 nm
514 nm
AMS dM/dlog10dva (µg m-3)
SMPS dM/dlog10dm (µg m-3)
AMS Org
AMS NO3
AMS SO4
AMS NH4
AMS Chl
SMPS
Vacuum aerodynamic diameter or mobility diameter (nm)

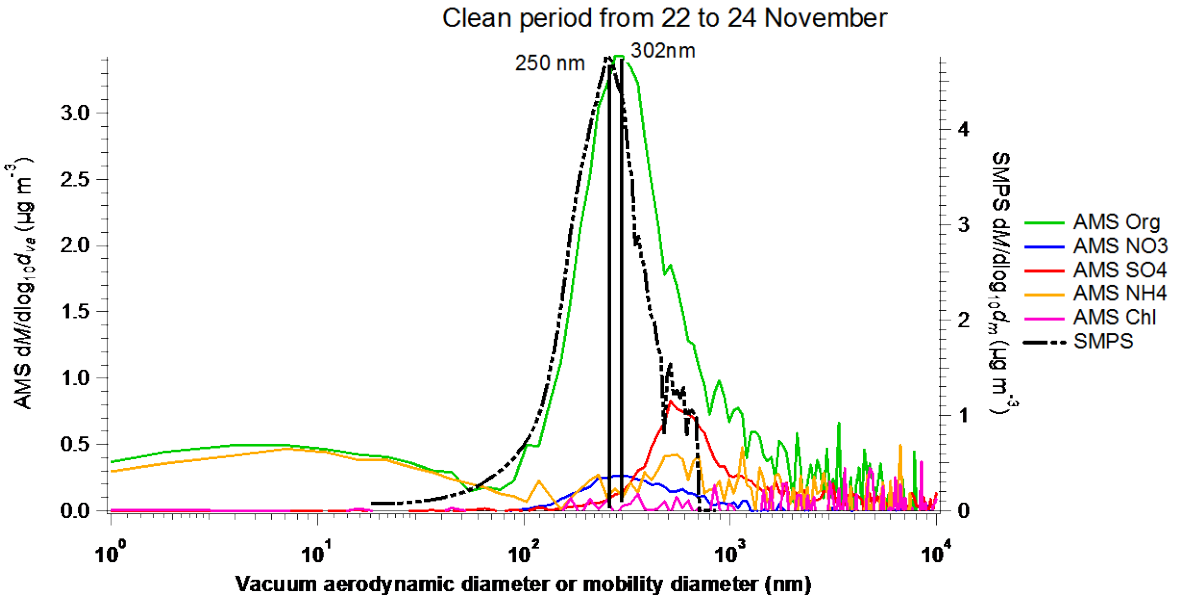
Clean period from 22 to 24 November
250 nm
302nm
AMS dM/dlog10dva (µg m-3)
SMPS dM/dlog10dm (µg m-3)
AMS Org
AMS NO3
AMS SO4
AMS NH4
AMS Chl
SMPS
Vacuum aerodynamic diameter or mobility diameter (nm)

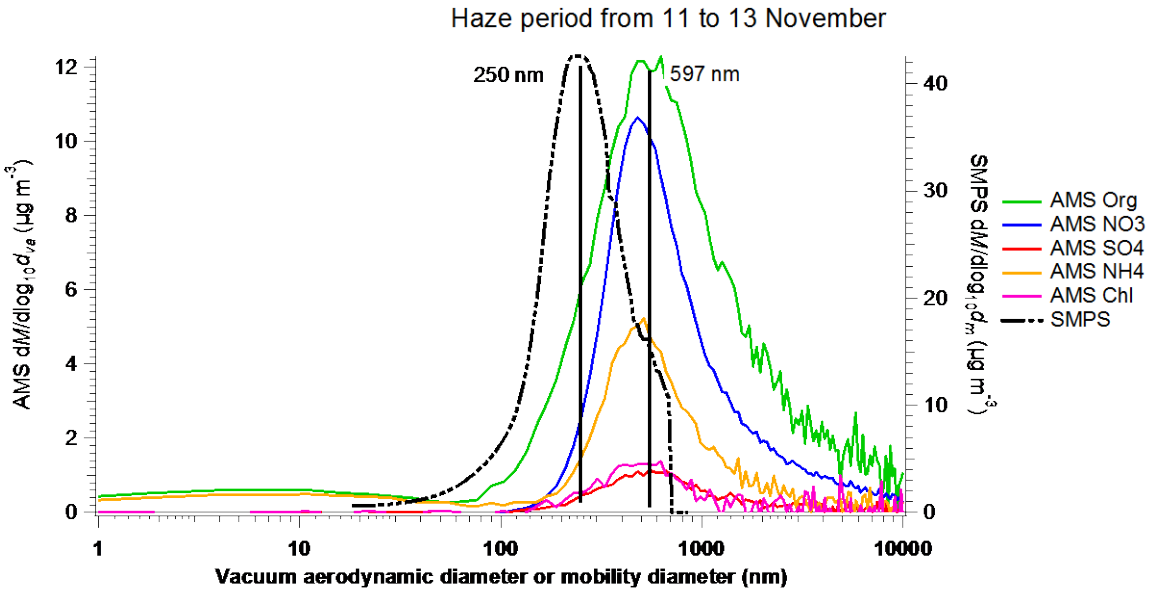
Haze period from 11 to 13 November
250 nm
597 nm
AMS dM/dlog10dva (μg m-3)
SMPS dM/dlog10dm (μg m-3)
Vacuum aerodynamic diameter or mobility diameter (nm)
AMS Org
AMS NO3
AMS SO4
AMS NH4
AMS Chl
SMPS

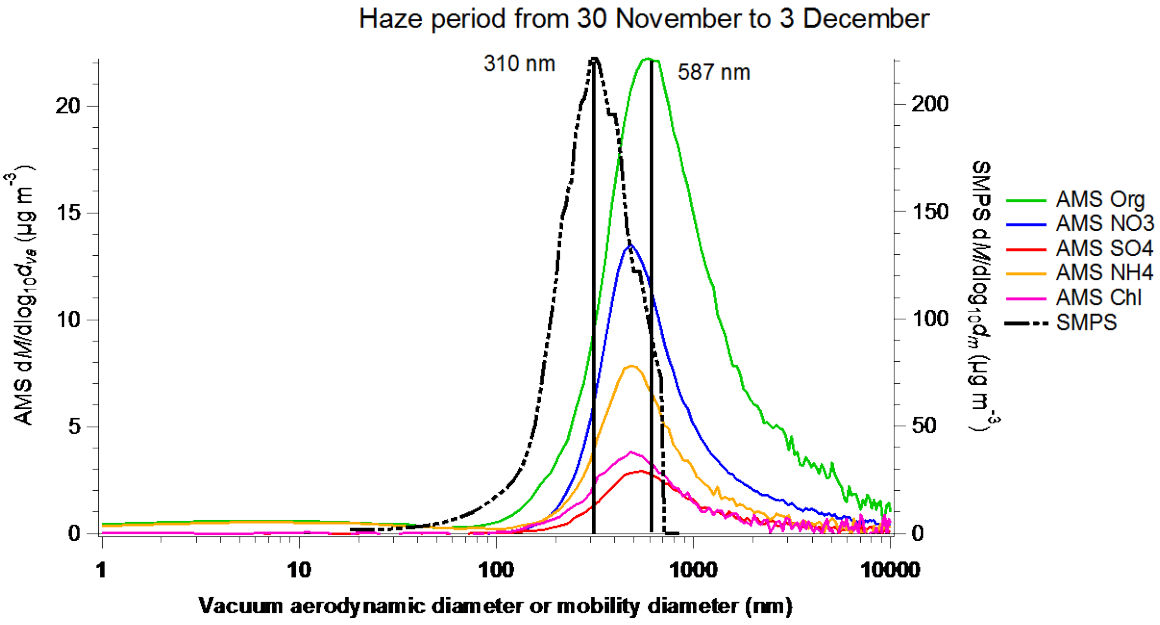
Haze period from 30 November to 3 December
310 nm
587 nm
AMS dM/dlog10dva (μg m-3)
SMPS dM/dlog10dm (μg m-3)
Vacuum aerodynamic diameter or mobility diameter (nm)
AMS Org
AMS NO3
AMS SO4
AMS NH4
AMS Chl
SMPS

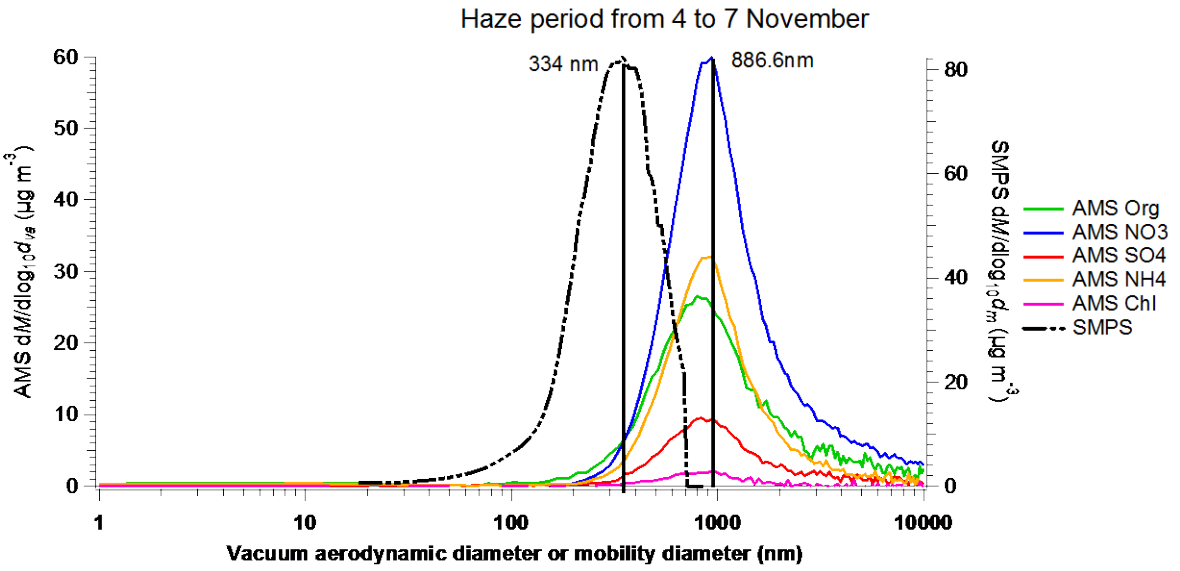

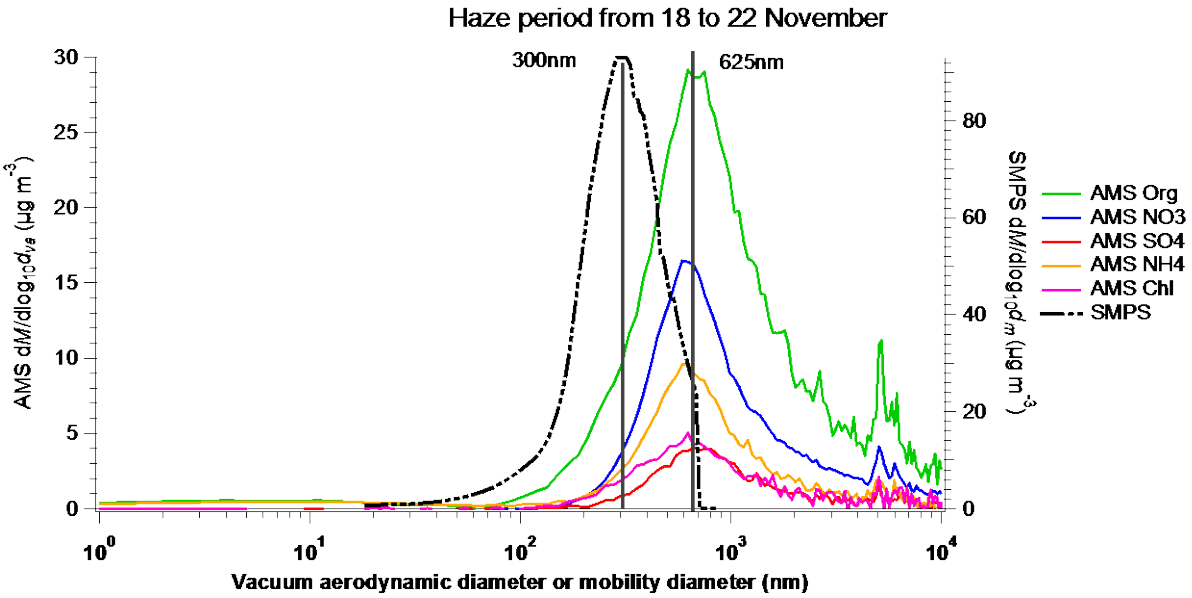

Comment #6

What is the difference in mass between the PM25 inlet and the SMPS. How representative of the total PM2.5 mass is the PM25 LTOFAMS measurements? Are auxiliary measurements of total PM available for comparison?

Response:

We have added a comparison of AMS NR-$PM_{2.5}$ and estimated SMPS mass (assuming an effective density of 1.2 g cm^{-3}) to the supplement as Fig. S4, and show the figure below for convenience.

The time series and scatter plot of particle concentration measured by AMS and SMPS are shown below and in Fig S4. As indicated in R2C4, the size cut of SMPS is 850 nm. The comparison between them shows three

distinct slopes in the scatter plot. The data from 31 Oct to 24 Nov falls mostly on the 1:1 line, except for the intense haze from 4 to 7 Nov, when the AMS concentration is much higher than the SMPS. This is because a large fraction of the mass occurs above the SMPS cutoff of 850 nm. After 25 Nov, we continue to observe a strong correlation between the SMPS and AMS, but is nearly 2 times higher than the AMS. This is believed to be a problem with the SMPS number counts. It is unlikely to be a problem with the AMS, as the correlation of $PM_{2.5}$ elemental sulphur measured by a co-located Xact and AMS sulphate is consistent throughout the study. This comparison is added to the supplement as Fig. S4 and shown below.

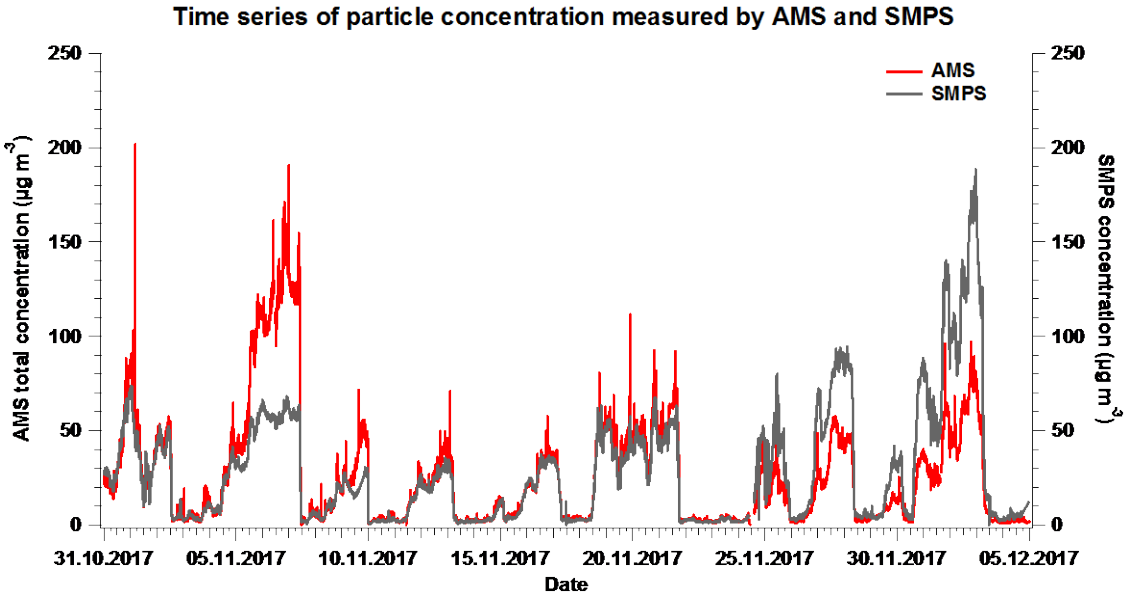

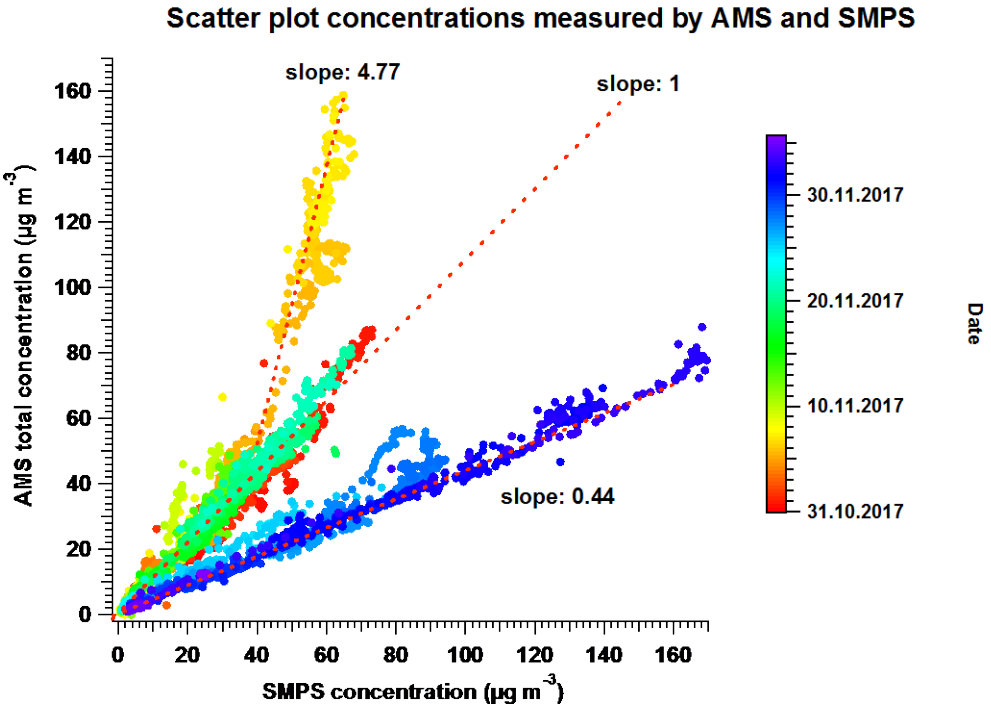

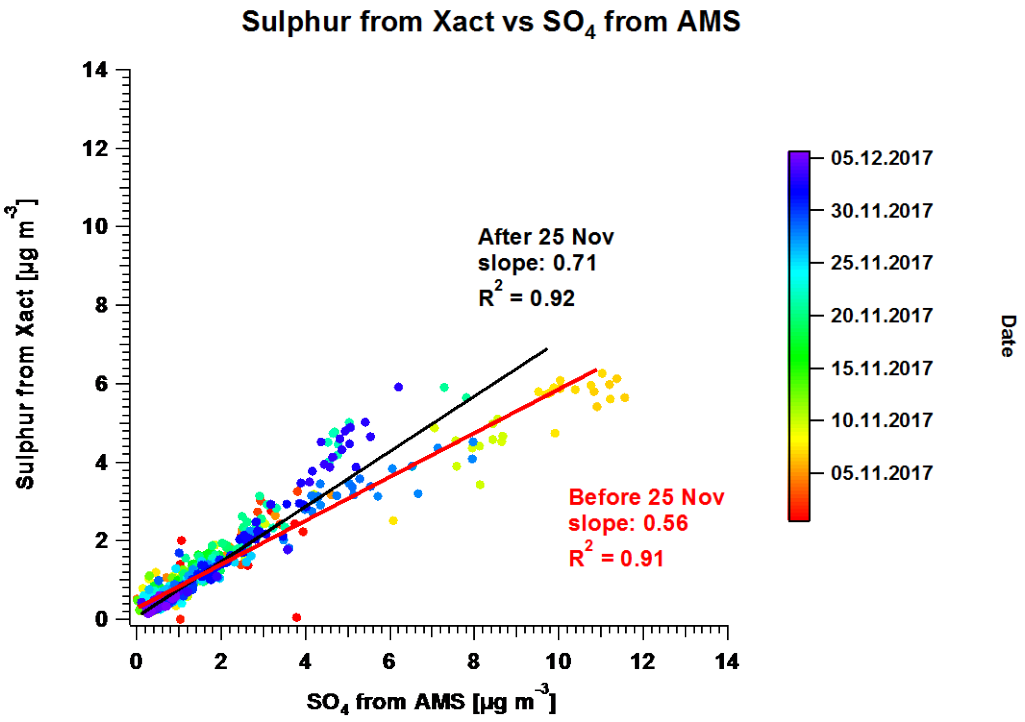

Comment #7

Given that the smaller, locally formed aerosol particles are not efficiently sampled by the PM25 inlet, what impact does this have on the interpretation of the measurements?

Response:

As shown by Xu et al. (2017), the $PM_{2.5}$ lens provides similar or better transmission to the standard PM_1 lens, except for d_{va} = 100-200 nm, where the $PM_{2.5}$ lens transmission is up to 50% lower. (Below 100 nm, the transmission decreases significantly but similarly for both lenses.) Assuming these particles are spherical and they have an effective density of 1.2 g cm^{-3}, this corresponds to a d_m range of 83 – 167 nm. As discussed in response to R2C4 and R2C5 and shown in Figs. S3 and S4, this accounts for a negligible mass fraction for all conditions encountered in the study. Therefore it is highly unlikely that these losses significantly affect the mass-based source apportionment analyses conducted here. However, given the lack of clearly multi-modal size distributions in the AMS, we cannot rule out the likelihood of an underestimation of all factors during clean periods rather than a bias in the fractional apportionment

Comment #8

Is a standard or capture vaporizer used in conjunction with the PM25 inlet? If a standard vaporizer is used, what is the particle collection efficiency estimated to be, and is the calculated CE dependent on particle diameters (to account for the enhanced effects of particle bounce for larger particles diameters)?

Response:

The original manuscript stated that the composition-dependent collection efficiency (CDCE) method was used (Middlebrook et al., 2012). We now also note that the AMS utilises a standard vaporizer, and no correction for large particles was applied. This is now stated in section 2.2 as follows (page 5 line 34):

"The particle beam impacts on a heated tungsten surface (standard AMS vaporiser, ~ 600 °C, and ~ 10^{-7} Torr)"

"A composition-dependent collection efficiency (CDCE) was applied to correct the measured aerosol mass (Middlebrook et al., 2012), and no size-dependent CE corrections were applied."

Comment #9

High concentrations were measured during this field campaign, often resulting in the clogging of the EESI-TOF instrument. Was there any evidence to suggest that there was overloading of the LTOFAMS instrument?

Response:

We did not find any evidence for clogging or overloading of the LTOF-AMS during the campaign. Throughout the entire campaign, the variation of the flowrate was <1 %. the airbeam < 10 %.

Comment #10

The authors show several PMF solution for the LTOFAMS analysis but only show the final solution for the EESI-TOF. Can the authors state if the PMF analysis on the "unconstrained" EESI TOF was performed? And if so which factors dominated the unconstrained PMF solution?

Response:

This is discussed in detail in response to R1C1, and we partially repeat the response here. Briefly, a preliminary PMF of the standalone EESI-TOF dataset was attempted but found to be uninterpretable, likely due to the suboptimal response of the EESI-TOF to the high concentrations experienced in this campaign, specifically denuder breakthrough. The PMF model requires detector linearity and static factor profiles, both of which are compromised by denuder breakthrough, because the volatile and semivolatile contributions to factor profiles depend on the time-dependent state of the denuder. Denuder breakthrough effects have recently been characterised in detail by Brown et al. (2021). As discussed in sections 2.2.1 and Text S3, we have tried to reduce these effects by removing ions likely to be dominated by gas phase/denuder breakthrough, but this method does not allow quantitative correction of signals from ions having contributions from both phases. However, by constraining the EESI-TOF PMF solution with AMS factor profiles, the solution becomes weighted towards explaining temporal trends observed in the particle phase. Further, by utilising the EESI-TOF for qualitative (factor identification) rather than quantitative (factor resolution) purposes, we minimise the effects of artifacts introduced by gaseous signals.

Comment #11

Aqueous phase SOA: The PMF analysis allowed the extraction of a more oxidized aqueous phase aerosol. In Fig. 3a the MOOA_AQ is shown to have highest concentrations (reaching 20 micrograms) during the haze event on the 4th and 7th, during high NO3 contributions (and high RH and low wind seed). The characteristic enhancement of the CO2 is illustrated in Fig. 7a during this period. However, there are several other periods during the field campaign when this MO-OOAaq species is identified (at concentrations near to 5 micrograms) (under the same conditions of RH and high NO3 Fraction) but the enhancement of the CO2+ signal was not observed. Is this CO2+ enhancement really associated with these species or is it somehow an artefact during high NO3 concentrations?

Response:

The reviewer identifies two important issues: (1) whether the enhanced CO_2^+/CO^+ signal can be a measurement artefact due to high NO_3^+ concentrations and (2) the reasons for the lack of enhancement in CO_2^+/CO^+ during periods of detectable MO-OOA_{aq} outside the 4-7 Nov. event. We address these questions separately below.

Regarding CO_2^+ artefacts, it is known that exposure to NO_3^+ leads to an artefact of increased CO_2^+ signal in the AMS (Pieber et al., 2016). As noted in the original text, we corrected for this effect by characterising the contribution from CO_2^+ and CO^+ during NH_4NO_3 calibrations, in which the concentration of NH_4NO_3 ranges from 5 to 80 µg cm^{-3}. The result shows that the artefact of NH_4NO_3 induced CO_2^+ signal according to Pieber et al. (2016) to total CO_2^+ signal is less than 5 %.

Regarding the second question, although MO-OOA_{aq} is detected throughout the rest of the campaign, its percent contribution to OA does not exceed 10 % during clean periods. During these periods, the overall concentrations are low enough that the CO^+ signal is rather noisy. Figure S22 shows the time series of reconstructed CO_2^+ and CO^+, which is the cross product of the time series matrix (G) and CO_2^+ and CO^+ relative intensity in factor profile matrix (F). It shows high CO_2^+/CO^+ ratio during the haze event between 4 to 7 November and nearly 1:1 ratio during the other periods although the MO-OOA_{aq} concentration is not negligible there. Compared to Fig. 10, the lack of significant increase of CO_2^+/CO^+ is a consequence of the OA composition.

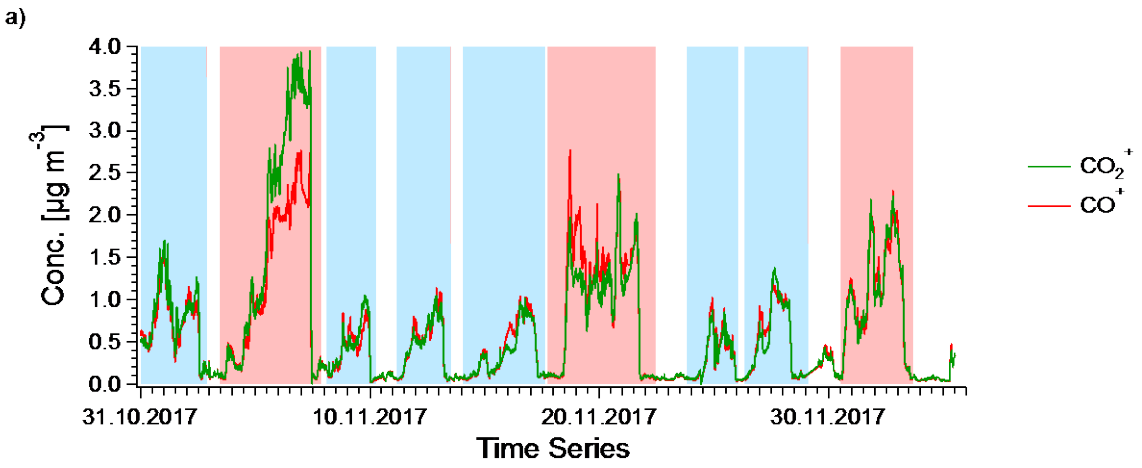

Comment #12

How did the factor mass spectral profile compare with reference mass spectra (oxalic acid, malonic acid and succinic acid (Canagaratna et al., 2015))?

Response:

The mass spectra of factor MO-OOA$_{aq}$ and MO-OOA$_{SFC}$, and malonic acid ($C_3H_4O_4$), oxalic acid ($C_2H_2O_4$) and succinic acid ($C_4H_6O_4$) are shown below and in Fig S21. The latter three species were measured with ammonium sulphate seeds under the environment of argon gas, therefore, huge peaks at m/z 18, 40 and 64 can be found. The ratio of CO_2^+/ CO^+ is 1.88, 1.34, 3.96, 1.69 and 0.56 for these five spectra, respectively. The acids are characterised by the $C_xH_yO_{z>1}$ group, and these ions have also although not outstanding, but high signal in the MO-OOA$_{aq}$ and MO-OOA$_{SFC}$ factors. Although MO-OOA$_{SFC}$ has also ions in this group, the ratio of CO_2^+/ CO^+ is much lower than the one of MO-OOA$_{aq}$.

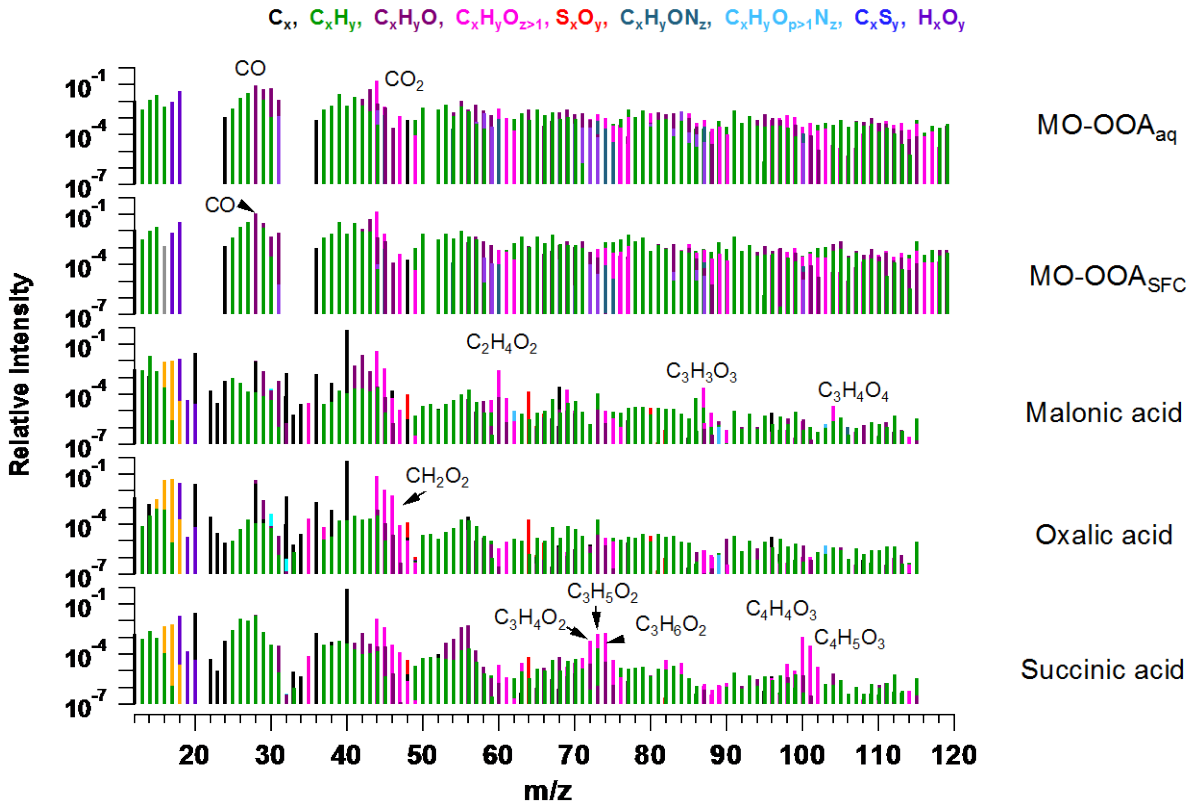

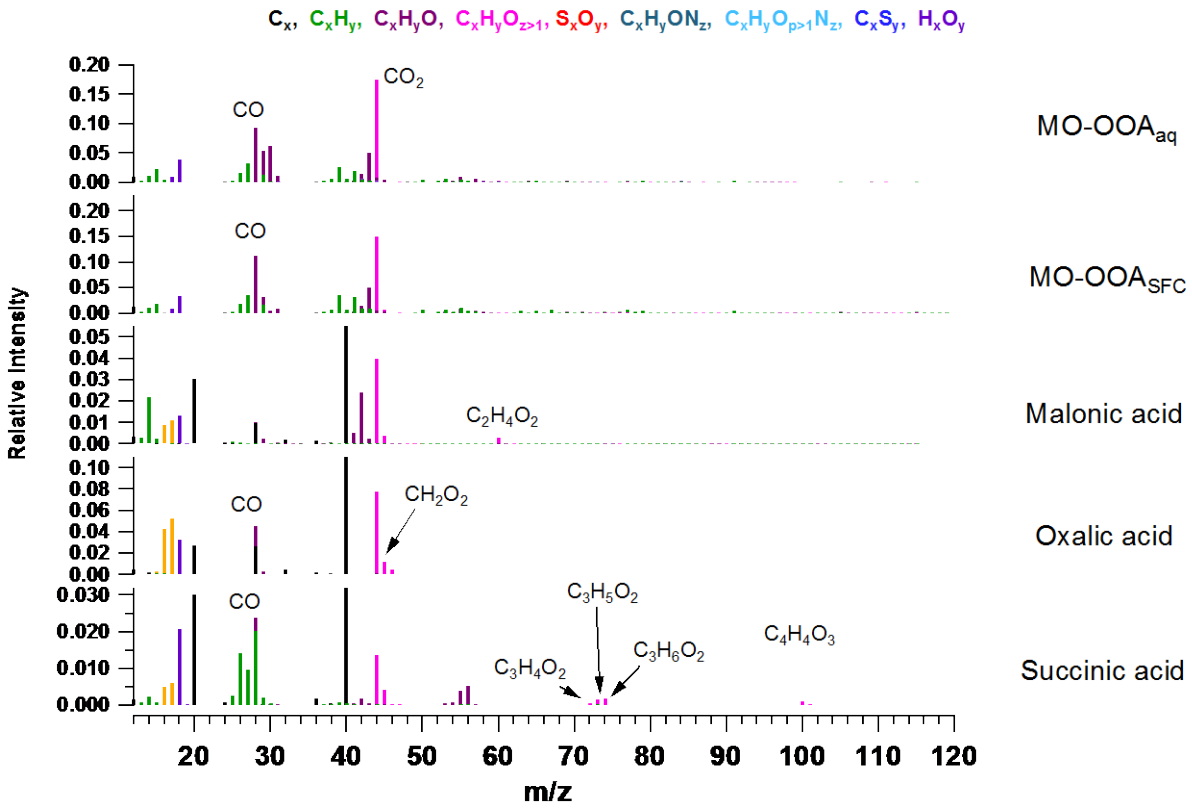

Comment #13

The authors state that the m/z 44 artefact is very low in this instrument (4%), however, could this CO2+ enhancement be somehow related to artefacts linked to mixtures of inorganic and organic species?

Response:

Pieber et al. (2016) investigated inorganic/organic mixtures, and showed that the artefact depended only on the inorganic fraction (nitrate and, to a lesser degree, sulphate). This has been further supported by the work of Freney et al. (2019) in investigations of laboratory and ambient aerosol.

Comment #14

Previous studies have shown how aerosol liquid water can promote the formation of water-soluble organic nitrogen (Yu Xu et al., 2020 Environ. Sci. Tech. https://pubs.acs.org/doi/pdf/10.1021/acs.est.9b05849). What is the role of nitrogen in the formation of these aqueous organic species? Is there evidence of organonitrate species? Has aerosol acidity being evaluated during these measurements (NOT measured, but can look at the ion balance)? During the intense haze episode, this MOOA species was measured continuously over a period of 3 days. In one of the cited articles (Kuang et al., 2020) it is mentioned that most of the aqSOA was formed during daytime periods with high photochemical activity and that dark aqSOA only contributed negligibly to the total OOA concentrations. In this work, the increase in aqSOA remains constant over three days with little

diurnal Variation. Do you consider that this aqSOA is locally formed or influenced by regional processes? Does the aerosol size distribution provide information to determine this?

Response:

As indicated in Fig. 11, the airmass passed through a high NO_x region, which provides an opportunity for inorganic nitrate formation homogeneously and/or heterogeneously, resulting in water uptake from the air and increased LWC concentration. Then this high LWC in turn facilitates further heterogeneous formation of nitrate. The high LWC also provides the environment for other aqueous phase chemistry.

Regarding organonitrates, *z*-score analysis of the MO-OOA_{aq} EESI-TOF profile identifies the nitrogen-containing species $C_9H_{15}NO_6$, $C_{10}H_{17}NO_5$ and $C_9H_{15}NO_5$ as ions characteristic of this factor, suspected to be organonitrates. The stack plots of these three ions in different factors and their contribution to total OA are shown below (also in Fig. S26). However, the organonitrate can be formed via aqueous phase chemistry and via gas phase reaction. From the EESI-TOF data alone, we cannot conclude that these organonitrates are only from aqueous phase chemistry.

From the AMS perspective, the ratio of NO^+ to NO_2^+ throughout the campaign is about 3.18, as shown in the first figure below (also in Fig. S23), whereas for the particular event from 4 to 7 Nov dominated by aqueous phase chemistry, the ratio is still about 3.13, as shown in the second scatter plot below. This ratio is close to the ratio of ammonium nitrate measured by the AMS from our IE calibration period (3.29) and from another study (3.5) (Sun et al., 2012), and much lower than the ratio of potassium nitrate (~28) (Drewnick et al., 2015). The NO_3^- concentration resulting from KNO_3 and $NaNO_3$ in this campaign is rather low, about 0.3 % (if we asume all K^+ and Na^+ coming from KNO_3 and $NaNO_3$), making an insignificant contribution to NO_3^- measured by the AMS. Considering the low ratio of NO^+ to NO_2^+ and the low contribution from KNO_3 and $NaNO_3$ to total NO_3^-, it is very likely that the ratio of NO^+ to NO_2^+ for this particular event from 4 to 7 Nov is governed by inorganic nitrate.

Regarding the time series for MO-OOA_{aq}, we calculated the change of the MO-OOA_{aq} concentration over time. The last figure in the reply to this comment (also shown in Fig. S24) shows the time series of MO-OOA_{aq} and the LWC in the upper panel, and the change of the MO-OOA_{aq} concentration over time (2 h time interval) in the lower panel. From the time series, no diurnal cycle for the haze event from 4 to 7 November is observed although there are some short periods when the MO-OOA_{aq} concentration decreases slightly, i.e., ΔMO-$OOA_{aq}/\Delta t < 0$. In addition, different from the MO-OOA_{aq} time series, the LWC concentration has a clear diurnal variation, as shown in Fig. 10. These observations are consistent with irreversible generation (as we suggest in the main text), although evaporation of reversibly-generated MO-OOA_{aq} that happens to be compensated for by a comparable increase in MO-OOA_{aq} production during the day cannot be completely ruled out.

As discussed in the text, the haze event featured by aqueous phase chemistry is considered to be both local and regional, because 1) the airmass passed through the high NO_x region resulting water uptake from the air and LWC concentration and on the way to Beijing, the airmass stayed long enough for aqueous phase chemistry to happen and 2) the stagnant condition in Beijing contributed to the accumulation of pollutants and haze formation. Therefore, we consider this event is considered as both locally and regionally influenced.

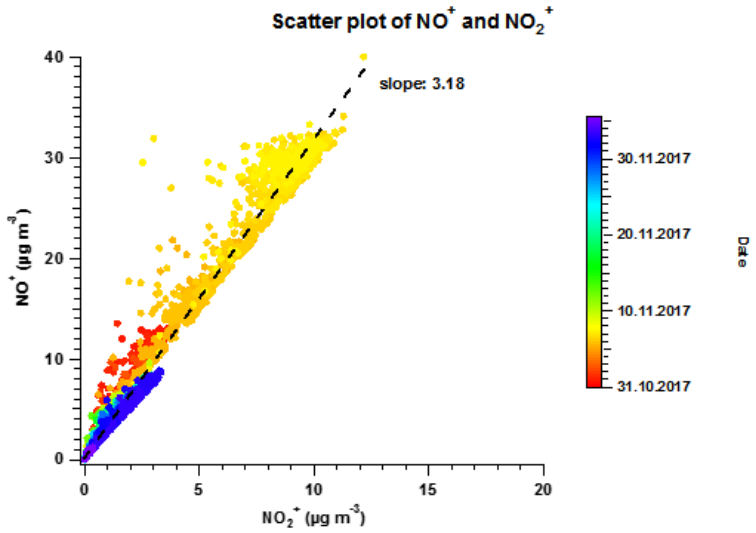
Scatter plot of NO+ and NO2+
slope: 3.18
NO+ (µg m-3)
NO2+ (µg m-3)
Date
30.11.2017
20.11.2017
10.11.2017
31.10.2017

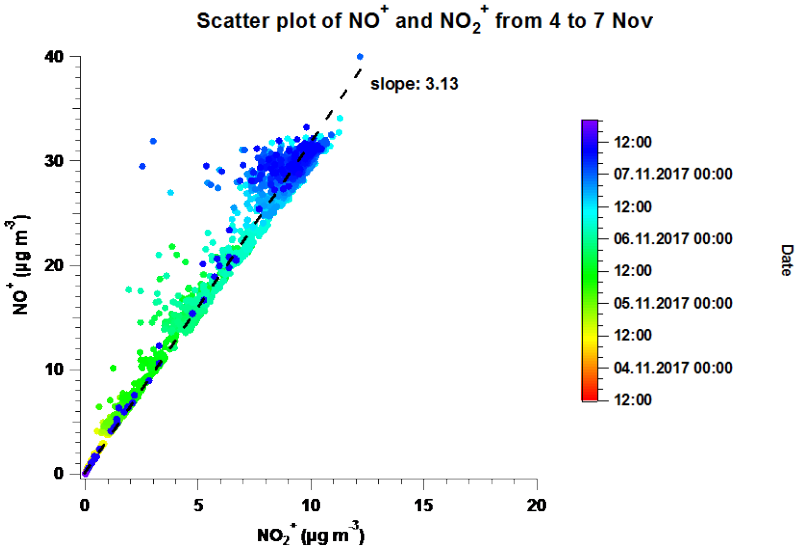
Scatter plot of NO+ and NO2+ from 4 to 7 Nov
slope: 3.13
NO+ (µg m-3)
NO2+ (µg m-3)
Date
12:00
07.11.2017 00:00
12:00
06.11.2017 00:00
12:00
05.11.2017 00:00
12:00
04.11.2017 00:00
12:00

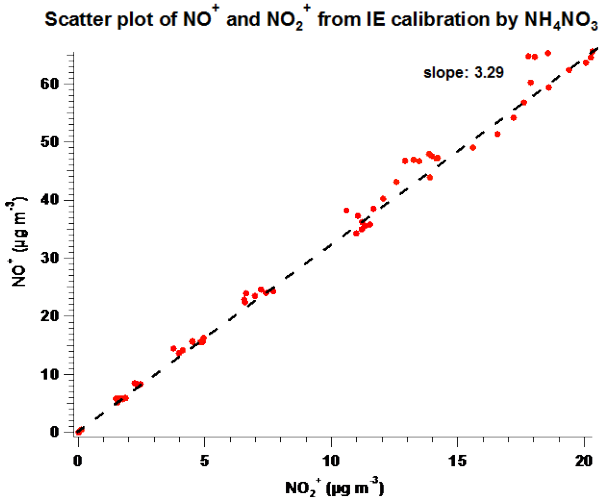
Scatter plot of NO+ and NO2+ from IE calibration by NH4NO3
slope: 3.29
NO+ (µg m-3)
NO2+ (µg m-3)

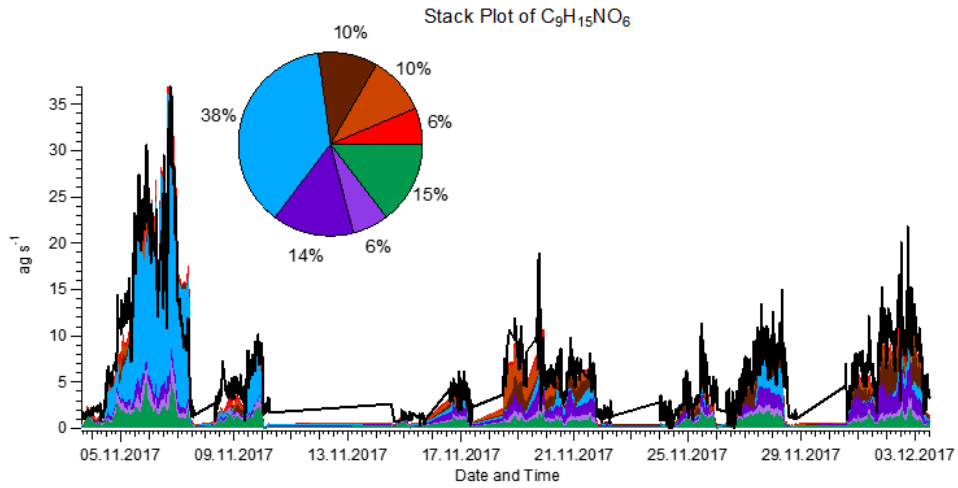
Stack Plot of $C_9H_{15}NO_6$
10%
10%
6%
15%
6%
14%
38%
ag s^{-1}
0
5
10
15
20
25
30
35
05.11.2017
09.11.2017
13.11.2017
17.11.2017
21.11.2017
25.11.2017
29.11.2017
03.12.2017
Date and Time

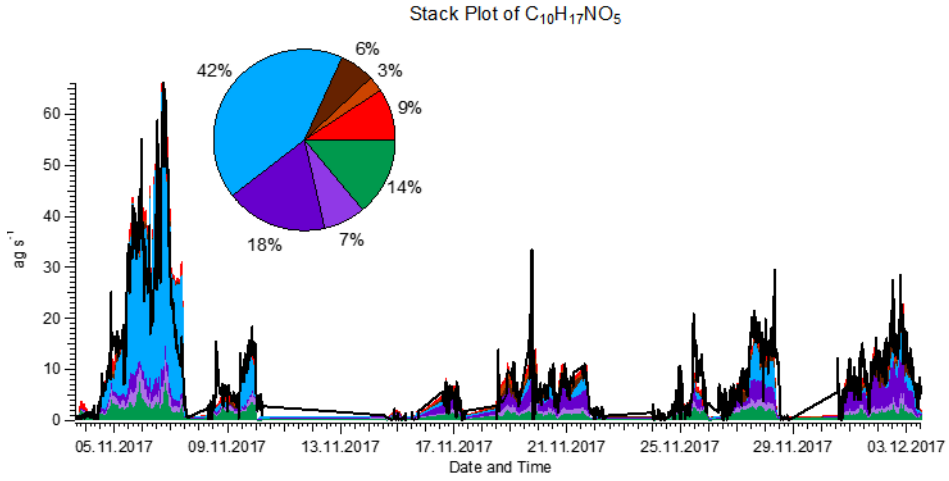
Stack Plot of $C_{10}H_{17}NO_5$
6%
3%
9%
14%
7%
18%
42%
ag s^{-1}
0
10
20
30
40
50
60
05.11.2017
09.11.2017
13.11.2017
17.11.2017
21.11.2017
25.11.2017
29.11.2017
03.12.2017
Date and Time

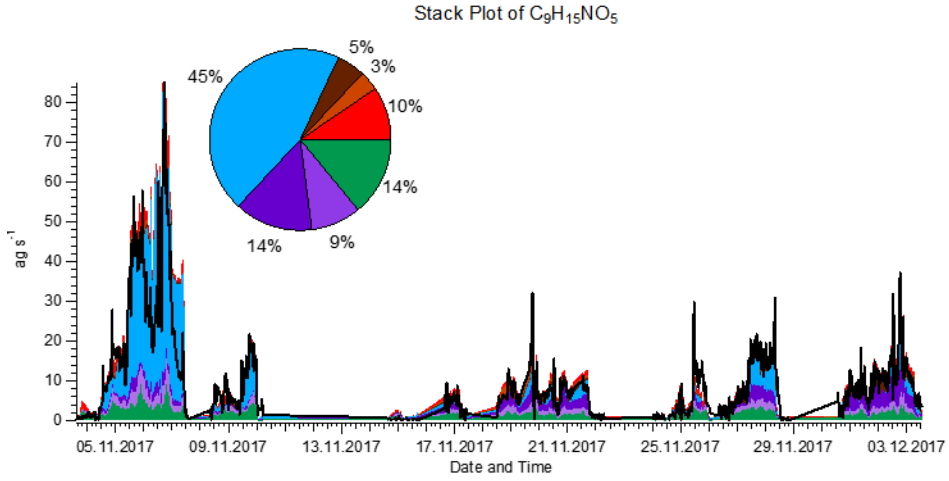
Stack Plot of $C_9H_{15}NO_5$
5%
3%
10%
14%
9%
14%
45%
ag s^{-1}
0
10
20
30
40
50
60
70
80
05.11.2017
09.11.2017
13.11.2017
17.11.2017
21.11.2017
25.11.2017
29.11.2017
03.12.2017
Date and Time

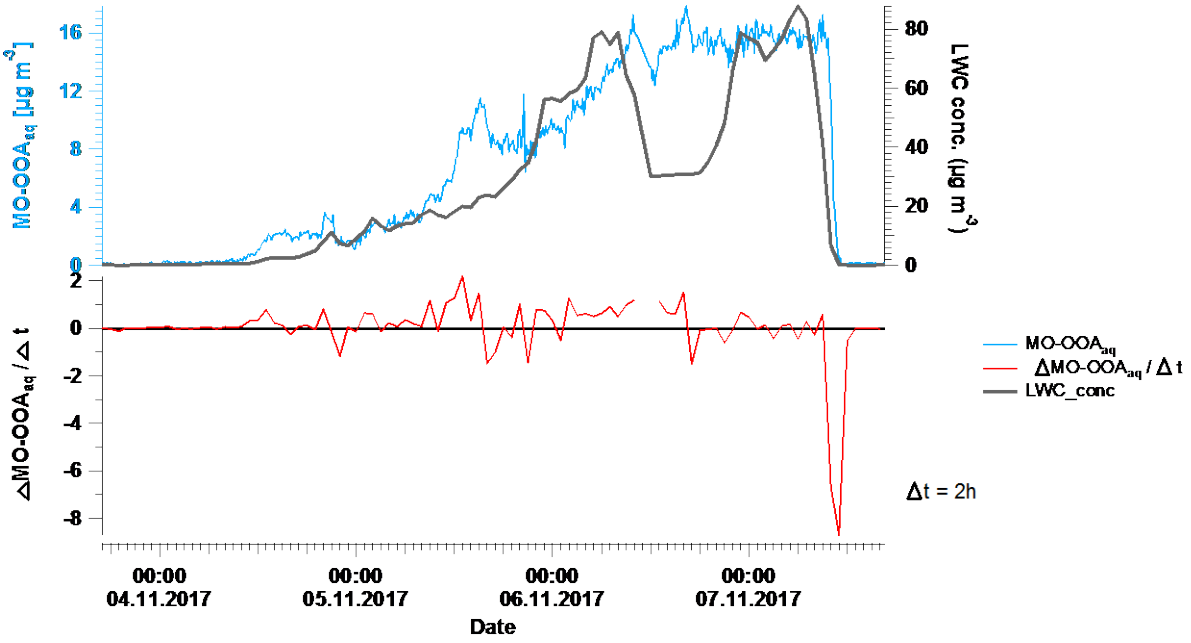

Comment #15

A non source-specific factor LO-OOA ns ?

Recently it has been shown that the PM25 inlet AMS systems may be capable of measuring airborne bacteria (Wolf et al., 2017 Atmospheric environment, (https://doi.org/10.1016/j.atmosenv.2017.04.001).). In this paper, there are some characteristics of the LO-OOAns species (O:C, diurnal pattern, higher concentrations during warm period than colder periods) as the resolved bacteria-like factor in Wolf et al.,2017. Is it possible to provide more information on the average diameter as a function of time for each of the resolved factors to help provide more information on their source and atmospheric processing prior to being sampled? At least provide the SMPS size distributions which would help illustrate regionally influenced factors and those from local processes.

Response:

We cannot conclusively provide time-dependent size distributions for each factor, but some rough estimates are possible.

We checked the explained variation of each ion in LO-OOA$_{ns}$. If the explained variation of one ion in this factor is higher than in any other factor and the unexplained part, we consider this ion to be a surrogate for the LO-OOA$_{ns}$ factor. There are $C_2H_3^+$, $C_3H_3^+$, $C_3H_6^+$, $C_4H_5^+$, $C_3H_9O_2^+$, $C_6H_6^+$ and $C_6H_{12}^+$. These ions have highest intensity and fractional contribution at the corresponding integer *m/z*, therefore, we use the integer *m/z* to represent each corresponding ion here. In addition, a high fraction of *m/z* 44 is also observed in this factor, which is a surrogate for secondary factors. Therefore, we plot the geometric mean diameter of size distribution of the integer *m/z* and *m/z* 44 at UMR as a function of time for all periods. For other factors, we use nitrate as a surrogate for MO-OOA$_{aq}$, and sulphate for other OOA factors, shown in the figures below and in Fig. S27.

In the minor haze events, from Fig 12, the contribution from LO-OOA$_{ns}$ is the highest among these resolved factors, however, the size distributions of these ions are comparable to their size distribution in the other

periods: 587 nm in minor haze events vs 839 nm in the major haze event from 4 to 7 Nov, 550 nm in the major haze event from 18 to 22 Nov and 625 nm in the major haze event from 30 Nov to 3 Dec.

We consider it very unlikely that the LO-OOA$_{ns}$ factor retrieved here is bacteria-related. There are major chemical differences between LO-OOA$_{ns}$ and the bacteria factor of Wolf et al. (2017). That study identified the bacteria OA based on ions in the C_xH_yN group at *m/z* 27, 30, 42, whereas in this paper, the surrogates for LO-OOA$_{ns}$ listed previously don't contain nitrogen. In addition, the bacteria factor is a minor faction (1.41 % in $PM_{2.5}$ and 0.52 % in PM_1) in Wolf et al. (2017), whereas in this paper, we observed high contribution of this LO-OOA$_{ns}$ factor during the haze events. Therefore, it is very unlikely that the LO-OOA$_{ns}$ is related to bacteria.

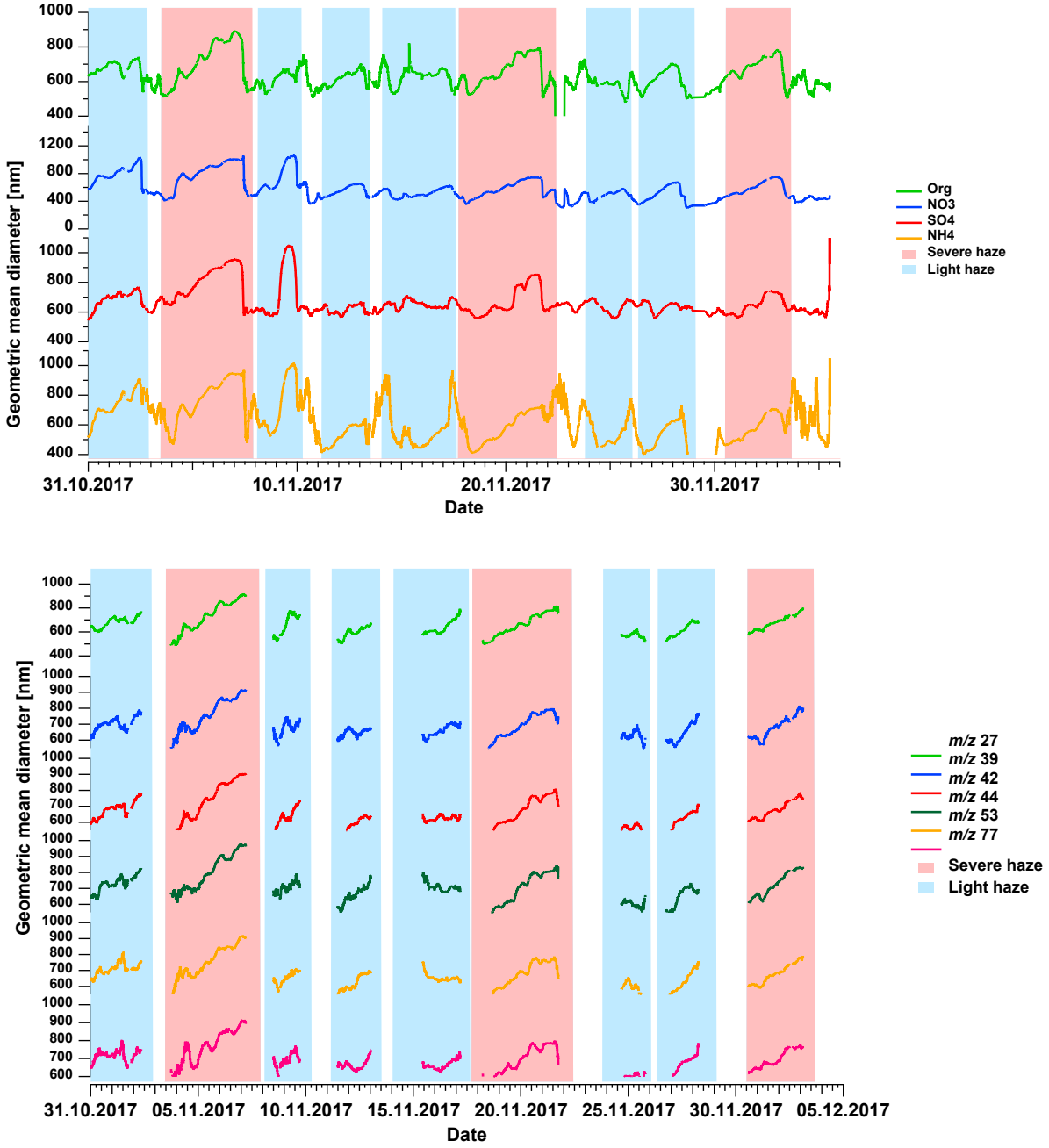

Comment #16

Were BC measurements available for correlation with the HOA and BBOA.

Response:

The equivalent black carbon (eBC) was measured by an aethalometer (model AE33, Magee Scientific). Here are the time series comparison and scatter plot (also in Fig. S16) between eBC and 1) HOA and 2) BBOA. Clearly, the correlation of eBC vs HOA is good, with a slope of 6.26 and $r^2 = 0.70$, consistent with the study from Poulain et al. (2021), but this slope is higher than the value typically reported in China (Zhu et al., 2018; Hu et al., 2016; Huang et al., 2010). The scatter plot of eBC vs BBOA is split into two period, 1) 18 to 19 Nov, the first two days of the haze event from 18 to 22 Nov and 2) rest of the campaign. The slope of the period 2) is 1.66, consistent with other studies (Poulain et al., 2021; Zhu et al., 2018) , whereas the slope in 1) gradually increases from 0.07 to 0.59, corresponding to the BBOA concentration decreasing from the beginning to the middle of this haze event.

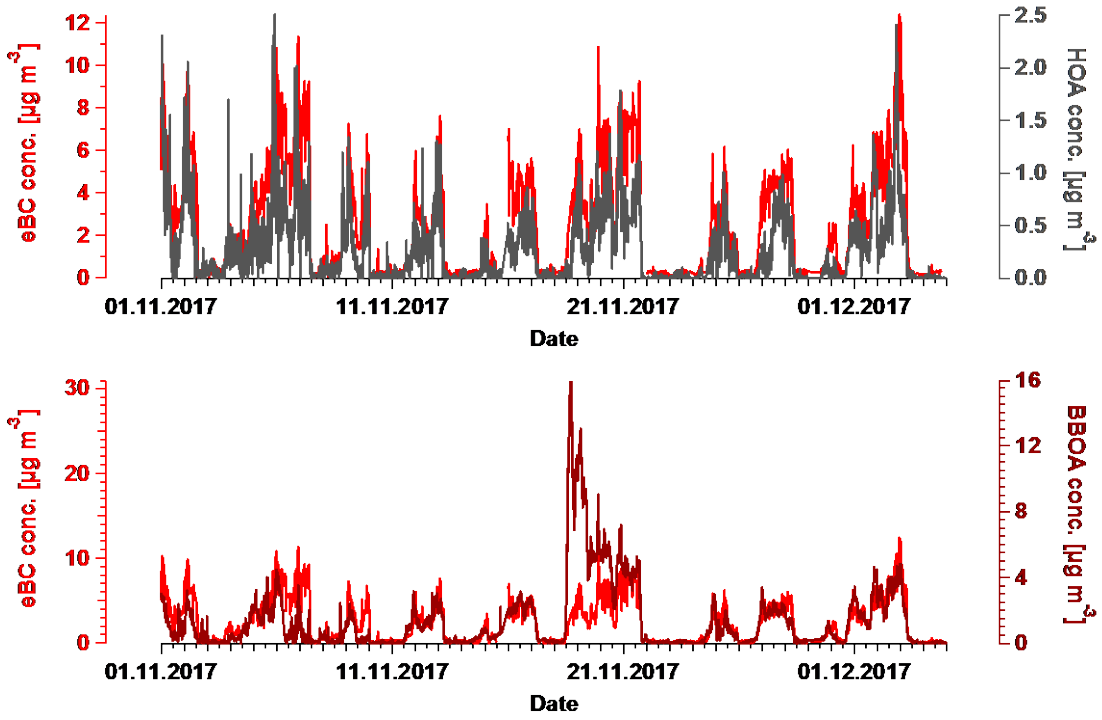

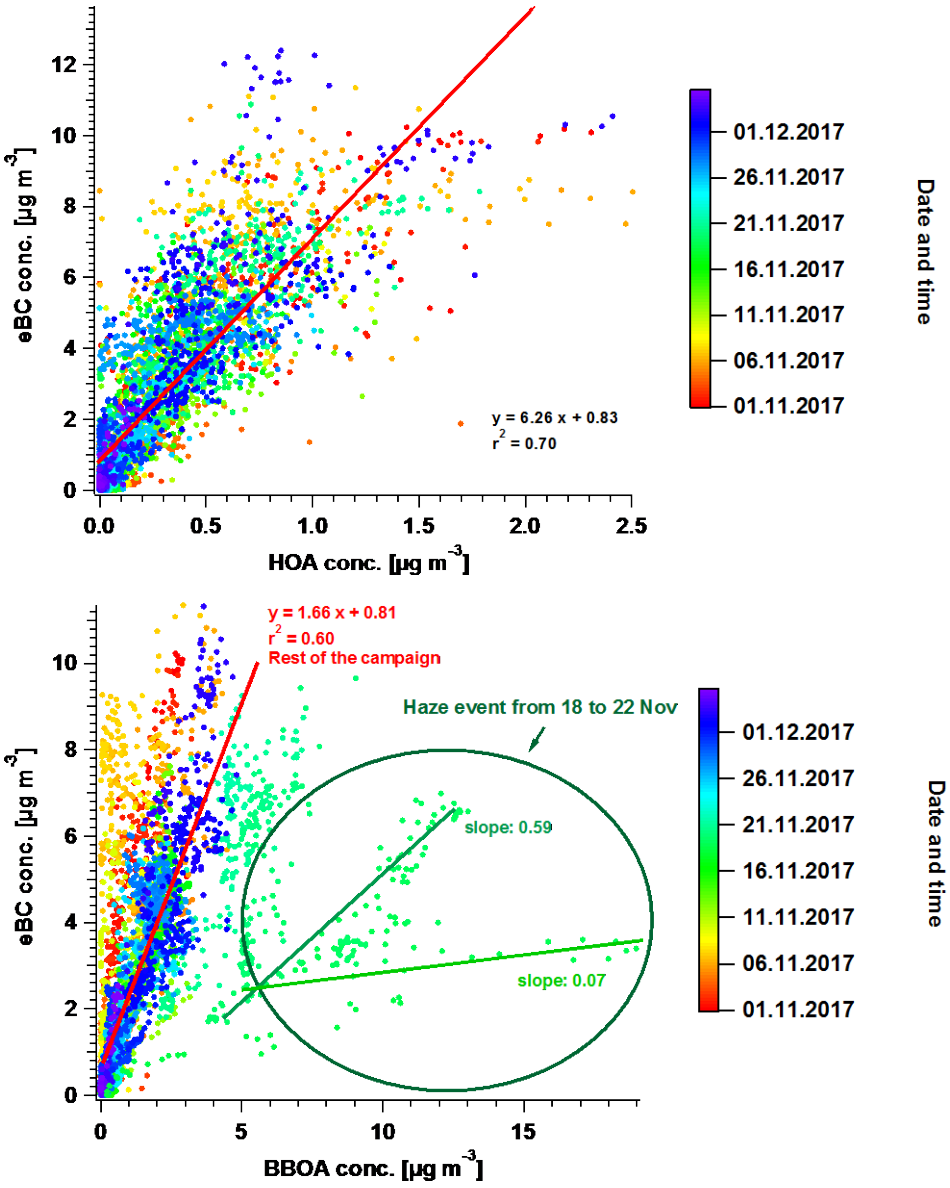

Comment #17 --- Minor remarks

When discussing the diurnal variations better referencing to the figure is necessary.

Response:

We now directly reference Fig. 3c wherever diurnal variations are in section 3.2

Comment #18 --- Minor remarks

Although the information of O/C, H/C are included in and Fig. 5 and 6, it would be useful for comparison to other studies, to have these average values as well as the N/C ratios illustrated on the factor profiles in Fig.3 and 4.

Response:

To avoid cluttering Fig. 3, we have added these values to the supplement in Table S1, the elemental ratio (H:C, O:C and N:C) for eight factors from AMS and seven factors from the EESI-TOF. The elemental ratio from AMS is calculated according to Canagaratna et al. (2015). For the EESI-TOF, the molecule-dependent sensitivity is not considered in the calculation.

	AMS			EESI		
	H:C	O:C	N:C	H:C	O:C	N:C
HOA	1.853 ± 0.009	0.022 ± 0.0003	0.006 ± 0.0002			
COA	1.629 ± 0.005	0.099 ± 0.001	0.003 ± 0.0001	1.755 ± 0.032	0.254 ± 0.058	0.008 ± 0.008
BBOA	1.419 ± 0.021	0.394 ± 0.023	0.022 ± 0.002	1.523 ± 0.061	0.426± 0.060	0.028 ± 0.007
CCOA	1.548 ± 0.017	0.155 ± 0.015	0.016 ± 0.001	1.569 ± 0.030	0.373± 0.022	0.017 ± 0.003
$MO\text{-}OOA_{aq}$	1.323 ± 0.018	0.576 ± 0.028	0.038 ± 0.005	1.659 ± 0.015	0.390± 0.009	0.030 ± 0.002
$MO\text{-}OOA_{SFC}$	1.220 ± 0.016	0.417 ± 0.013	0.011 ± 0.002	1.623 ± 0.026	0.354± 0.008	0.041 ± 0.005
$LO\text{-}OOA_{SFC}$	1.656 ± 0.031	0.246 ± 0.056	0.064 ± 0.013	1.662 ± 0.090	0.409± 0.107	0.023 ± 0.012
$LO\text{-}OOA_{ns}$	1.565 ± 0.011	0.134 ± 0.008	0.008 ± 0.0005	1.693 ± 0.022	0.334± 0.008	0.018 ± 0.003

Comment #19 --- Minor remarks

Page 13, Line 11: Were external time series available for comparison, other than CO? Can you provide the value for the "good" correlation.

Response:

The time series comparison and scatter plot of HOA vs. CO have been added to the supplement as Fig. S16. The slope in the scatter plot is 1332, consistent with the previous studies (Poulain et al., 2021; Zhang et al., 2017).

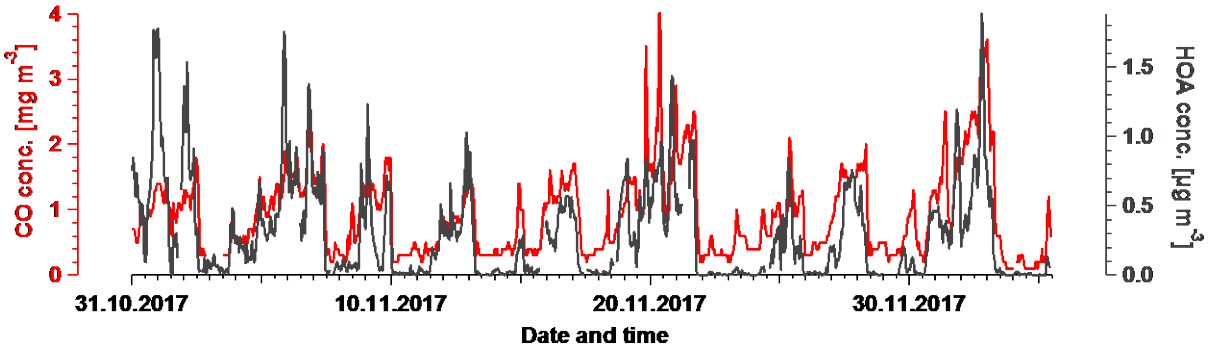

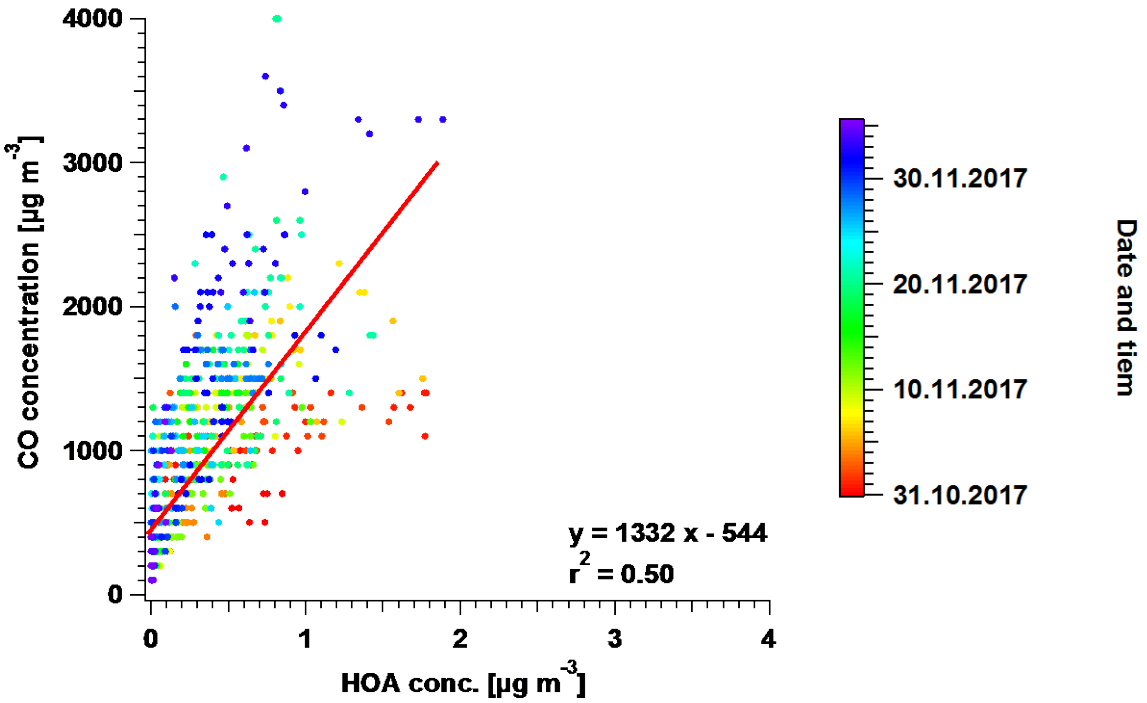

Comment #20 --- Minor remarks

Page 22, Line 44 (please include correct section no.)

Response:

This information was added to section 3.3.4 as following (page 14 line 41):

"Note that due to the application of the volatility-based filter for distinguishing particle-phase vs. spurious ions (see section Text S3), the contribution of such small, highly oxygenated ions presented here represents a lower limit."

Comment #21 --- Minor remarks

Page 23, Line 7 r2 =of 0.93), remove = or of

Response:

This typo was corrected (page 14 line 50):

"The LWC concentration is presented in Fig. 10, together with the time series of MO-OOA_{aq}. The two time series are strongly correlated (r^2 = 0.93), and both are dramatically higher during the 4 to 7 November event than for the rest of the study."

Comment #22 --- Minor remarks

Page 21, Line 25: Bertrand et al.. please include the full reference.

Response:

Because it is no longer clear when and in which form this data will be published, and a detailed discussion of this complex environmental campaign is beyond the scope of the current manuscript, the reference has been changed in the reference list:

Bertrand, A., personal communication.

Comment #23 --- Minor remarks

Page 5, Line10 What is this diagnostic species?

Response:

This question was also raised by Reviewer 1 (R1C16) and we repeat the response here. The sentence in question was meant to introduce the need to identify a diagnostic species, the identity (AMS NO_3^+) and use of which comprise the rest of the paragraph. To clarify this, the revised sentence reads (page 3 line 11 in supplement, as suggested by R1C19, we move this part to Text S4 in supplement):

"Therefore, we select a diagnostic species that can be measured with higher time resolution is utilised to monitor the sensitivity throughout the campaign."

Comment #24 --- Minor remarks

Is the custom peak fitting algorithm something that could be applied to lower resolution instruments in the future?

Response:

This is an interesting question, and one that we hope to explore in the future. In our view, a prerequisite for its routine use in spectral analysis would be a robust validation on synthetic data, which we have not yet conducted. Therefore we do not recommend it for widespread use (at the present time) and consider its use here as an *ad hoc* adaptation to sub-optimal instrument performance, with the lack of systematic validation increasing the uncertainties and informing our decision to utilise the EESI-TOF data for interpretative (qualitative) analysis rather than quantitative factor resolution (see also response to R1C1).

Reference

Brown, W. L., Day, D. A., Stark, H., Pagonis, D., Krechmer, J. E., Liu, X., Price, D. J., Katz, E. F., DeCarlo, P. F., Masoud, C. G., Wang, D. S., Hildebrandt Ruiz, L., Arata, C., Lunderberg, D. M., Goldstein, A. H., Farmer, D. K., Vance, M. E., and Jimenez, J. L.: Real-time organic aerosol chemical speciation in the indoor environment using extractive electrospray ionization mass spectrometry, Indoor Air, 31, 141-155, https://doi.org/10.1111/ina.12721, 2021.

Canagaratna, M. R., Jimenez, J. L., Kroll, J. H., Chen, Q., Kessler, S. H., Massoli, P., Hildebrandt Ruiz, L., Fortner, E., Williams, L. R., Wilson, K. R., Surratt, J. D., Donahue, N. M., Jayne, J. T., and Worsnop, D. R.: Elemental ratio measurements of organic compounds using aerosol mass spectrometry: characterization, improved calibration, and implications, Atmos Chem Phys, 15, 253-272, https://doi.org/10.5194/acp-15-253-2015, 2015.

Drewnick, F., Diesch, J. M., Faber, P., and Borrmann, S.: Aerosol mass spectrometry: particle–vaporizer interactions and their consequences for the measurements, Atmos. Meas. Tech., 8, 3811-3830, https://doi.org/10.5194/amt-8-3811-2015, 2015.

Elser, M., Huang, R. J., Wolf, R., Slowik, J. G., Wang, Q. Y., Canonaco, F., Li, G. H., Bozzetti, C., Daellenbach, K. R., Huang, Y., Zhang, R. J., Li, Z. Q., Cao, J. J., Baltensperger, U., El-Haddad, I., and Prevot, A. S. H.: New insights into PM2.5 chemical composition and sources in two major cities in China during extreme haze events using aerosol mass spectrometry, Atmos Chem Phys, 16, 3207-3225, https://doi.org/10.5194/acp-16-3207-2016, 2016.

Freney, E., Zhang, Y. J., Croteau, P., Amodeo, T., Williams, L., Truong, F., Petit, J. E., Sciare, J., Sarda-Esteve, R., Bonnaire, N., Arumae, T., Aurela, M., Bougiatioti, A., Mihalopoulos, N., Coz, E., Artinano, B., Crenn, V., Elste, T., Heikkinen, L., Poulain, L., Wiedensohler, A., Herrmann, H., Priestman, M., Alastuey, A., Stavroulas, I., Tobler, A., Vasilescu, J., Zanca, N., Canagaratna, M., Carbone, C., Flentje, H., Green, D., Maasikmets, M., Marmureanu, L., Minguillon, M. C., Prevot, A. S. H., Gros, V., Jayne, J., and Favez, O.: The second ACTRIS inter-comparison (2016) for Aerosol Chemical Speciation Monitors (ACSM): Calibration protocols and instrument performance evaluations, Aerosol Sci Tech, 53, 830-842, https://doi.org/10.1080/02786826.2019.1608901, 2019.

Hu, W. W., Hu, M., Hu, W., Jimenez, J. L., Yuan, B., Chen, W. T., Wang, M., Wu, Y. S., Chen, C., Wang, Z. B., Peng, J. F., Zeng, L. M., and Shao, M.: Chemical composition, sources, and aging process of submicron aerosols in Beijing: Contrast between summer and winter, J Geophys Res-Atmos, 121, 1955-1977, https://doi.org/10.1002/2015JD024020, 2016.
Huang, X. F., He, L. Y., Hu, M., Canagaratna, M. R., Sun, Y., Zhang, Q., Zhu, T., Xue, L., Zeng, L. W., Liu, X. G., Zhang, Y. H., Jayne, J. T., Ng, N. L., and Worsnop, D. R.: Highly time-resolved chemical characterization of atmospheric submicron particles during 2008 Beijing Olympic Games using an Aerodyne High-Resolution Aerosol Mass Spectrometer, Atmos Chem Phys, 10, 8933-8945, https://doi.org/10.5194/acp-10-8933-2010, 2010.

Lee, C.P., Surdu, M., Bell, D., Lamkaddam, H., Wang, M., Ataei, F., Hofbauer, V., Lopez, B., Donahue, N., Dommen, J., Prevot, A. S. H., Slowik, J. G., Wang, D., Baltensperger, U., and El-Haddad, I.: Effects of aerosol size and coating thickness on the molecular detection using extractive electrospray ionization, Atmos. Meas.Tech., submitted, 2021.

Pieber, S. M., El Haddad, I., Slowik, J. G., Canagaratna, M. R., Jayne, J. T., Platt, S. M., Bozzetti, C., Daellenbach, K. R., Frohlich, R., Vlachou, A., Klein, F., Dommen, J., Miljevic, B., Jimenez, J. L., Worsnop, D. R., Baltensperger, U., and Prevot, A. S. H.: Inorganic Salt Interference on CO2+ in Aerodyne AMS and ACSM Organic Aerosol Composition Studies, Environ Sci Technol, 50, 10494-10503, https://doi.org/10.1021/acs.est.6b01035, 2016.

Poulain, L., Fahlbusch, B., Spindler, G., Müller, K., van Pinxteren, D., Wu, Z., Iinuma, Y., Birmili, W., Wiedensohler, A., and Herrmann, H.: Source apportionment and impact of long-range transport on

carbonaceous aerosol particles in central Germany during HCCT-2010, Atmos. Chem. Phys., 21, 3667-3684, https://doi.org/10.5194/acp-21-3667-2021, 2021.

Sun, Y. L., Zhang, Q., Schwab, J. J., Yang, T., Ng, N. L., and Demerjian, K. L.: Factor analysis of combined organic and inorganic aerosol mass spectra from high resolution aerosol mass spectrometer measurements, Atmos. Chem. Phys., 12, 8537-8551, https://10.5194/acp-12-8537-2012, 2012.

Williams, L. R., Gonzalez, L. A., Peck, J., Trimborn, D., McInnis, J., Farrar, M. R., Moore, K. D., Jayne, J. T., Robinson, W. A., Lewis, D. K., Onasch, T. B., Canagaratna, M. R., Trimborn, A., Timko, M. T., Magoon, G., Deng, R., Tang, D., Blanco, E. D. L. R., Prevot, A. S. H., Smith, K. A., and Worsnop, D. R.: Characterization of an aerodynamic lens for transmitting particles greater than 1 micrometer in diameter into the Aerodyne aerosol mass spectrometer, Atmos Meas Tech, 6, 3271-3280, https://doi.org/10.5194/amt-6-3271-2013, 2013.

Wolf, R., El-Haddad, I., Slowik, J. G., Dällenbach, K., Bruns, E., Vasilescu, J., Baltensperger, U., and Prévôt, A. S. H.: Contribution of bacteria-like particles to PM2.5 aerosol in urban and rural environments, Atmospheric Environment, 160, 97-106, https://doi.org/10.1016/j.atmosenv.2017.04.001, 2017.

Xu, W., Croteau, P., Williams, L., Canagaratna, M., Onasch, T., Cross, E., Zhang, X., Robinson, W., Worsnop, D., and Jayne, J.: Laboratory characterization of an aerosol chemical speciation monitor with PM2.5 measurement capability, Aerosol Sci Tech, 51, 69-83, https://doi.org/10.1080/02786826.2016.1241859, 2017.

Zhang, X., Zhang, Y., Sun, J., Yu, Y., Canonaco, F., Prévôt, A. S. H., and Li, G.: Chemical characterization of submicron aerosol particles during wintertime in a northwest city of China using an Aerodyne aerosol mass spectrometry, Environmental Pollution, 222, 567-582, https://doi.org/10.1016/j.envpol.2016.11.012, 2017.

Zhu, Q., Huang, X. F., Cao, L. M., Wei, L. T., Zhang, B., He, L. Y., Elser, M., Canonaco, F., Slowik, J. G., Bozzetti, C., El-Haddad, I., and Prévôt, A. S. H.: Improved source apportionment of organic aerosols in complex urban air pollution using the multilinear engine (ME-2), Atmos. Meas. Tech., 11, 1049-1060, https://doi.org/10.5194/amt-11-1049-2018, 2018.